Directing the Deposition of Ferromagnetic Cobalt onto Pt-Tipped CdSe@CdS Nanorods: Synthetic and Mechanistic Insights

Lawrence J. Hill,[†] Mathew M. Bull,[†] Younghun Sung,[‡] Adam G. Simmonds,[†] Philip T. Dirlam,[†,§] Nathaniel E. Richey,[†] Sean E. DeRosa,[†] In-Bo Shim,[⊥] Debanjan Guin,[†] Philip J. Costanzo,[§] Nicola Pinna,[‡,∥] Marc-Georg Willinger,[#] Walter Vogel,[△] Kookheon Char,[‡] and Jeffrey Pyun[†,‡,*]

[†]Department of Chemistry and Biochemistry, University of Arizona, 1306 E. University Boulevard, Tucson, Arizona 85721, United States , [‡]World Class University Program for Chemical Convergence for Energy and Environment, Department of Chemical and Biological Engineering, Seoul National University, Seoul 151-744, Korea, [§]Department of Chemistry, California Polytechnic University, San Luis Obiso, California, United States, [⊥]Department of Nano and Electronic Physics, Kookmin University, Seoul, 136-702, Korea, [∥]Department of Chemistry and CICECO, University of Aveiro, Campus Universitario de Santiago, 3810-193, Averio, Portugal, [#]Department of Inorganic Chemistry, Fritz Haber Institute of the Max Planck Society, Berlin, Germany, and [△]Department of Chemistry, National Central University, Taiwan

ABSTRACT A methodology providing access to dumbbell-tipped, metal—semiconductor and metal oxide—semiconductor heterostructured nanorods has been developed. The synthesis and characterization of CdSe@CdS nanorods incorporating ferromagnetic cobalt nanoinclusions at both nanorod termini (*i.e.*, dumbbell morphology) are presented. The key step in the synthesis of these heterostructured nanorods was the decoration of CdSe@CdS nanorods with platinum nanoparticle tips, which promoted the deposition of metallic CoNPs onto Pt-tipped CdSe@CdS nanorods. Cobalt nanoparticle tips were then selectively oxidized to afford CdSe@CdS nanorods with cobalt oxide domains at both termini. In the case of longer cobalt-tipped nanorods, heterostructured nanorods were observed to self-organize into complex dipolar assemblies, which formed as a consequence of magnetic associations of terminal CoNP tips. Colloidal polymerization of these cobalt-tipped nanorods afforded fused nanorod assemblies from the oxidation of cobalt nanoparticle tips at the ends of nanorods *via* the nanoscale Kirkendall effect. Wurtzite CdS nanorods survived both the deposition of metallic CoNP tips and conversion into cobalt oxide phases, as confirmed by both XRD and HRTEM analysis. A series of CdSe@CdS nanorods of four different lengths ranging from 40 to 174 nm and comparable diameters (6—7 nm) were prepared and modified with both cobalt and cobalt oxide tips. The total synthesis of these heterostructured nanorods required five steps from commercially available reagents. Key synthetic considerations are discussed, with particular emphasis on reporting isolated yields of all intermediates and products from scale up of intermediate precursors.

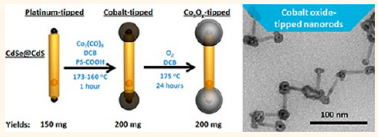

KEYWORDS: heterostructured nanorods · dipolar assembly · ferromagnetic nanoparticles · CdSe@CdS · colloidal polymerization

Heterostructured nanocrystals composed of semiconductor and metallic colloids have generated considerable interest as a route to prepare nanocomposites with controllable placement of disparate nanoinclusions and electronically coupled interfaces.[1−3] These materials are of particular interest in photoelectrochemical energy and photocatalysis, as charge transfer processes can be directed across nano-Schottky, or p−n junctions.[4−23] Recent advances in synthetic colloid chemistry have enabled the preparation of a wide range of heterostructured nanorods,[24−38] heterodimeric nanoparticles,[39−52] core−shell colloids,[8−11,42−44,53−59] and coated 1-D nanomaterials.[30,60−62] Heterostructured colloids composed of semiconductor nanorods tipped with magnetic[63−68] or noble materials[19−21,68−77] in either "matchstick" or "dumbbell" topologies have received recent attention as a route to well-defined 1-D nanocrystals. The seminal work of Banin *et al.* demonstrated the preparation of dumbbell heterostructured nanorods by the tipping of CdSe nanorods with various terminal metal nanoparticles (NPs).[76−79] Mokari *et al.* further expanded on the scope of these materials by the incorporation metal NP tips (Au, Pt, Pd, *etc.*) onto extended CdSe and CdS nanorods.[66,69] Cozzoli and Manna *et al.* demonstrated the preparation of heterostructured nanorods by the combination of a wide range of materials based on Au, CdS, CdSe, TiO_2, metallic Co, iron oxides, and CdSe@CdS seeded nanorods.[64,65,71] In general, these approaches utilized a preformed semiconductor nanorod precursor, which was then used to selectively seed the growth of disparate nanoparticle tips requiring appropriate matching of the colloidal components and determination of optimal conditions.

Incorporation of cobalt nanoparticles (CoNPs) into colloidal semiconductor heterostructures was first demonstrated by the

* Address correspondence to jpyun@email.arizona.edu.

Received for review May 4, 2012 and accepted August 17, 2012.

Published online August 18, 2012
10.1021/nn3019859

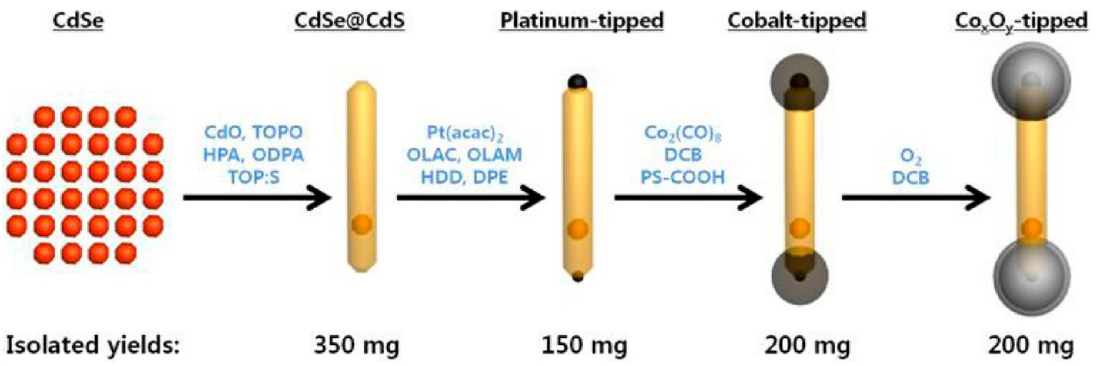

Scheme 1. Five-step synthesis of Co_xO_y-tipped nanorods with dumbbell morphology. CdSe quantum dot seeds (D = 2.3−2.7 nm) were used to form heterostructured CdSe@CdS nanorods of varying length (40−174 nm). PtNP deposition onto CdSe@CdS nanorod termini was then conducted for the series of CdSe@CdS nanorods to enable cobalt deposition. Selective oxidation of cobalt-tipped nanorods afforded the final product. Isolated yields for each intermediate and the final product are listed above. Abbreviations: (TOPO) trioctylphosphine oxide, (TOP) trioctylphosphine, (HPA) *n*-hexylphosphonic acid, (ODPA) *n*-octadecylphosphonic acid, (OLAC) oleic acid, (OLAM) oleylamine, (HDD) 1,2-hexadecanediol, (DPE) diphenyl ether, (PS-COOH) carboxylic acid-terminated polystyrene, (DCB) 1,2-dichlorobenzene.

direct deposition of terminal metal NP tips onto nanorod precursors. Soulantica and co-workers treated CdSe nanorods with cobaltocene complexes under an H_2 atmosphere to deposit a single CoNP onto the CdSe nanorod.[67] Cozzoli *et al.* exposed CdSe@CdS nanorods to a surfactant-free environment chosen to etch and activate nanorod termini for Co deposition.[64] When conducted in the presence of cobalt precursors, this etching step resulted in activation of the sulfur-rich nanorod termini with concomitant deposition of a single CoNP tip on each nanorod. The absence of ligands or a coordinating solvent combined with tight control of reactant concentrations over time (*via* syringe pump delivery of $Co_2(CO)_8$) was essential in driving the formation of Co tips and suppression of self-nucleation of unattached free CoNPs. Optimization resulted in asymmetric Co-tipping at one terminus of each rod (matchstick morphology) with high fidelity.

Earlier reports demonstrated the use of noble metal NPs as seeds for the overcoating of cobalt metal and metal oxides to form core−shell NPs.[80−83] Kim *et al.* reported that ligand-capped AuNPs served as efficient seeds for the preparation of dipolar core−shell Au@CoNPs using polymeric ligands.[84] Given the extensive reports on the deposition of noble metals (*e.g.*, Au, Pt) onto the terminal ends of semiconductor nanorods (*e.g.*, CdS, CdSe@CdS, CdSe),[1,66,76,77,79,85,86] numerous combinations of materials can be utilized to promote deposition of other metals (*e.g.*, Fe, Co) onto semiconductor nanorods. Recently, Chan *et al.* reported the deposition and simultaneous oxidation of FeNP tips onto Au-tipped CdSe@CdS nanorods in a dumbbell type morphology, which clearly demonstrated the advantages of using noble metal tips on CdSe@CdS nanorods to promote the deposition of magnetic colloidal shells.[68]

Herein, we demonstrate the synthesis of CdSe@CdS nanorods with magnetic cobalt domains at both termini (dumbbell morphology). Modification of CdSe@CdS nanorods was chosen (*versus* CdS or CdSe nanorods) due to the enhanced photoelectrochemical and photocatalytic properties reported for these heterostructured nanorods.[4] Terminal cobalt domains were then selectively oxidized to afford Co_xO_y-tipped nanorods without degradation of the CdSe@CdS nanorod (Scheme 1). Native CdSe@CdS nanorods decorated with PtNP tips enabled the selective deposition of metallic cobalt nanoparticles (CoNPs) as a colloidal shell around PtNP tips, providing an efficient methodology to incorporate CoNPs onto CdSe@CdS nanorods at both nanorod termini. The mechanistic aspects of PtNP-tip deposition onto CdSe@CdS nanorods are discussed, as this key modification was essential for selective deposition of cobalt and cobalt oxide nanoinclusions at both termini. In this multistep synthesis, dicobaltoctacarbonyl ($Co_2(CO)_8$) was used as the CoNP precursor, since this reagent was commercially available and amenable to conditions employed for cobalt deposition reactions.

Furthermore, this report focuses on the synthetic aspects of the total synthesis of these heterostructured nanorods, where highly detailed experimental procedures are included in the Supporting Information. A fundamental challenge in the field of nanoparticle chemistry pertains to the small reaction scales typically utilized to prepare inorganic nanomaterials. This often leads to omission of basic, critical information, such as isolated yields of intermediates and products, which impedes reproduction of reported synthetic methods. This issue for this report was obviated by developing conditions to scale up the preparation of key intermediates, enabling isolated yields in the range of 100−350 mg. To our knowledge, this level of synthetic detail has not been reported for these types of colloids and is an important step to facilitate wider utilization of these synthetic methods by the materials chemistry community.[52,87]

RESULTS AND DISCUSSION

CdSe@CdS Nanorods. Ligand-capped CdSe@CdS nanorods were prepared using a modified method from Manna *et al*.,[28] where CdSe quantum dots (diameter = 2.3−2.7 nm) were used to seed the growth of nanorods of varying length (nanorod length (L) = 40 ± 4, 77 ± 10, 126 ± 13, 174 ± 19 nm; population of sampled rods (n) = 100 for size distribution analysis). This series of CdSe@CdS nanorods all possessed comparable nanorod diameters (nanorod diameter (D) = 6−7 nm). Increasing the scale and isolated yields of CdSe@CdS nanorods was a crucial development to enable access to sufficient quantities of material to complete the total synthesis. Synthetic modifications to currently published methods were developed that enabled isolated yields of 300−350 mg for all nanorod lengths (see Supporting Information, Section 1c, Table S1).

Platinum-Tipped CdSe@CdS Nanorods. The deposition of metallic PtNPs onto the termini of CdSe@CdS nanorods was conducted onto a series of nanorod precursors with varying lengths (40−174 nm). The incorporation of PtNP tips onto CdSe@CdS nanorods proved to be a critical step to enable efficient deposition of metallic CoNPs onto semiconductor nanorods. A modified method from Mokari *et al*. was used to prepare nanorods consisting of the hot injection of $Pt(acac)_2$ and CdSe@CdS nanorods (1:1 wt ratio) into diphenyl ether containing 1,2-hexadecanediol, oleic acid, and oleylamine at 225 °C.[66] The deposition of PtNP tips onto CdSe@CdS nanorods appeared to be independent of nanorod length, enabling application of similar conditions for the series of CdSe@CdS nanorods. Mixtures of one sided PtNP-tipped nanorods (matchsticks) and two-sided PtNP-tipped nanorods (dumbbells) were formed. This mixture was found to be sufficient to drive the nearly quantitative formation of CoNP-tipped dumbbells after treatment with $Co_2(CO)_8$.

Initially, it was anticipated that the formation of PtNP tips on both ends of CdSe@CdS nanorods would be necessary to promote selective deposition of CoNP tips onto both nanorod termini. Earlier work by Banin *et al*. revealed that under air-free conditions preferential deposition of a single AuNP tip onto a CdS nanorod terminus occurred onto the sulfur-rich face of the nanorod to form matchstick-tipped nanorods.[79] This study further indicated that two-sided, AuNP-tipped CdS dumbbell nanorods could be formed under aerobic conditions *via* etching of Cd-rich nanorod faces by reagents/ligands used in the AuNP deposition reaction, which activated both termini for AuNP tip deposition. However, in this report, longer reaction times also resulted in the lateral deposition of AuNPs. Hence, anaerobic conditions were chosen to avoid lateral decoration of nanorods with PtNPs, and an excess of $Pt(acac)_2$, oleylamine, and oleic acid under argon were used to promote deposition of PtNP tips onto both ends of the nanorod. It was anticipated under these conditions that the initial deposition of the first PtNP tip would occur onto sulfur-rich lattice facets, followed by chemical etching of the cadmium-rich lattice facets to deposit the second PtNP tip to form dumbbell-type nanorods.[70,79,86] However, despite the addition of excess $Pt(acac)_2$, ligands, and 1,2-hexadecanediol relative to CdSe@CdS nanorods, a mixture of nanorods containing both one-sided matchsticks and two-sided PtNP dumbbell morphologies was observed from low-resolution TEM (Figure 1).

High-resolution TEM (HRTEM) indicated the presence of polycrystalline PtNP tips with particle diameters in the range 2−5 nm (Figure 1) of varying contrast. A survey of the gross morphology of a small population of heterostructured nanorods (124 nanorods: L = 45 ± 3 nm; D = 7 ± 1 nm) from TEM revealed the formation of one-sided Pt-tipped CdSe@CdS matchstick nanorods as the major product (60%) with a significant fraction of two-sided Pt-tipped CdSe@CdS dumbbell nanorods (38%) and a small portion of unmodified CdSe@CdS nanorods (2%). A significant excess of free, ligand-capped PtNPs was also formed and subsequently removed by precipitation of Pt-tipped nanorods in a mixed solvent system of toluene/EtOH (3.5:1) followed by centrifugation (Supporting Information, Section 1d). Short reaction times of 8 min were used despite affording both Pt-tipped matchstick and dumbbell nanorods since these mixtures were sufficient to enable selective and high-yielding two-sided deposition of metallic CoNP tips in the subsequent step. Dimensional changes in nanorods were not observed under the conditions and reaction times used in the Pt deposition step.

Cobalt- and Cobalt Oxide-Tipped Nanorods. As noted earlier, cobalt deposition reactions directly onto CdSe@CdS nanorods were unsuccessful and hence required pretreatment with PtNP tips (see Supporting Information, Figure S17). Therefore, cobalt deposition reactions using mixtures of both one- and two-sided Pt-tipped nanorods (four separate reactions with parent nanorod lengths from 40 to 174 nm) were conducted *via* the thermolysis of $Co_2(CO_8)$ in the presence of carboxylic acid terminated polystyrene (PS-COOH) ligands. For all nanorod lengths, nearly quantitative two-sided deposition of metallic CoNP tips on the termini of Pt-tipped CdSe@CdS nanorods was observed. Surprisingly, the predominant formation of dumbbell-tipped nanorods with CoNPs at each terminus was observed by TEM despite the apparent distribution of PtNP tips (dumbbell, matchstick, and unmodified nanorods, Figure 2).

In the synthesis of CoNP-tipped nanorods, isolated PtNP-tipped CdSe@CdS nanorods of lengths 40, 77, 126, and 174 nm were dispersed in DCB containing PS-COOH ligands (M_n = 12,500; M_w/M_n = 1.14) prepared by atom transfer radical polymerization. After

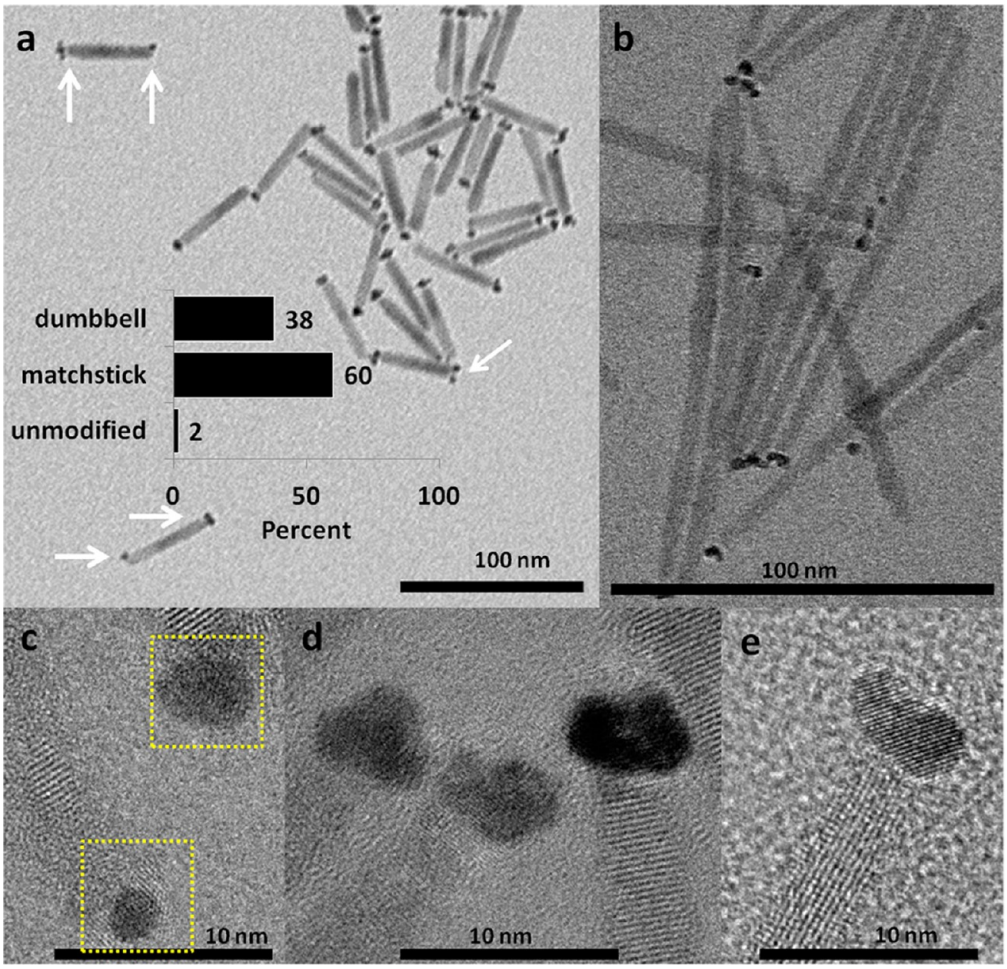

Figure 1. Asymmetrically platinum-tipped CdSe@CdS nanorods. (a) Arrows direct the reader to the variety of asymmetric Pt-tip morphologies found in a representative sample (nanorods: $L = 45 \pm 3$ nm; $D = 7 \pm 1$ nm; $n = 100$). The inset graph shows the relative percentages of doubly, singly, and untipped nanorods (38:60:2, respectively, based on 124 heterostructures examined). (b–e) HRTEM of Pt-tipped nanorods (nanorods: $L = 126 \pm 13$ nm; $D = 7 \pm 1$ nm; $n = 100$). Dumbbell Pt-tipped nanorods were observed to have different sized tips on each end, as shown in c (boxes are 5 nm square). Irregularly shaped Pt tips were far more common than spherical tips. Scale bars: a, b, 100 nm; c–e, 10 nm.

heating to 173 °C, a room-temperature solution of dicobaltoctacarbonyl ($Co_2(CO)_8$) in DCB was then injected into the mixture, resulting in a temperature drop to 160 °C, which was maintained until the end of the reaction. Using these conditions, the diameter of CoNP tips was found to be in the range 12–19 nm regardless of nanorod length, where the products exhibited a dumbbell-type morphology. At feed ratios of 10:1 by weight of $Co_2(CO)_8$ to PtNP-tipped CdSe@CdS matchstick and dumbbell nanorods, selective growth of CoNPs was observed to proceed onto the tips of CdSe@CdS nanorods, without the formation of free CoNPs (Figure 2a–d). Consequently, higher feed ratios of $Co_2(CO)_8$ to PtNP-tipped CdSe@CdS (*e.g.*, 12:1 by wt) resulted in CoNP deposition onto nanorod tips with concomitant growth of free CoNPs, where free, unbound CoNPs were stabilized by PS-COOH ligands. Additionally, we observed selective Co deposition onto nanorod tips for Pt-tipped CdSe@CdS nanorods with lengths below 100 nm (Figure 2a,b), while longer nanorods (126 and 174 nm) resulted in both terminal deposition of CoNP tips and lateral deposition along the length of the CdSe@CdS nanorods. Cozzoli *et al.* observed similar trends for CdSe@CdS nanorods in this size regime, where the deposition of metallic CoNPs was observed exclusively on the sides of nanorods with bare nanorod termini still exposed.[64] To explore the possibility of suppressing lateral deposition of metallic CoNPs along the length of nanorods, a separate batch of Pt-tipped CdSe@CdS nanorods ($L = 156 \pm 20$ nm, $n = 100$; with both matchstick and dumbbell PtNP morphologies) was prepared and then treated with $Co_2(CO)_8$ and PS-COOH at lower feed ratios (6:1 by wt). From these conditions CoNP tips (16 ± 2 nm, $n = 100$) were deposited almost exclusively onto both ends of Pt-tipped nanorods, with a very small fraction of laterally decorated CoNPs, demonstrating the enhanced flexibility in synthetic conditions afforded by using PtNP tips to seed formation of CoNP tips. Interestingly, we observed self-organization of these

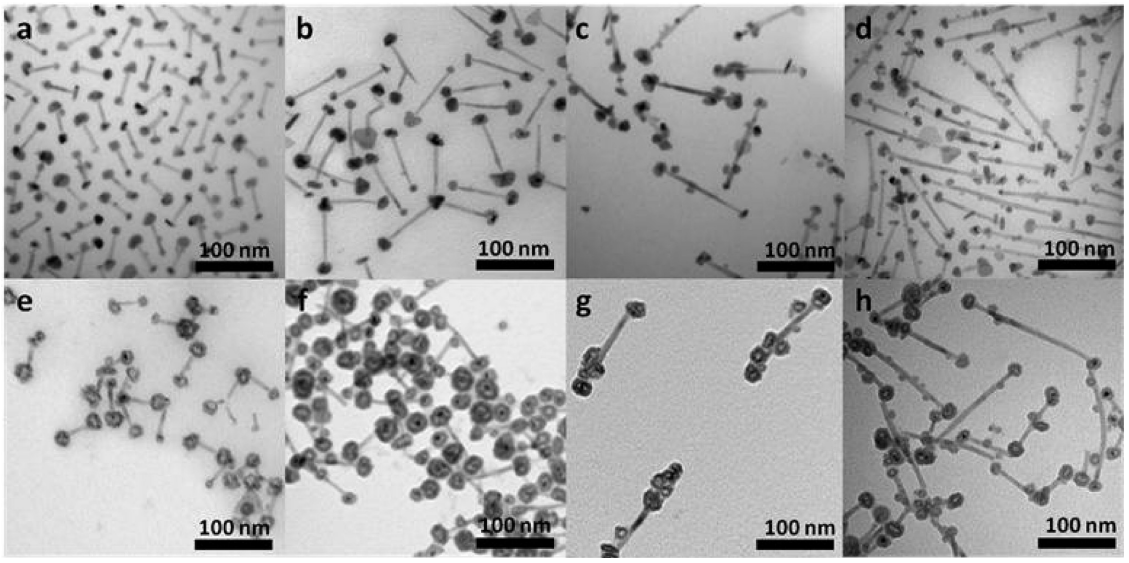

Figure 2. (a–d) Four lengths of cobalt-tipped nanorods with dumbbell morphology before (a–d) and after (e–h) the selective oxidation of cobalt. Nanorod dimensions: (a, e) $L = 40 \pm 4$ nm, $D = 6 \pm 1$ nm; (b, f) $L = 77 \pm 10$ nm, $D = 6 \pm 1$ nm; (c, g) $L = 126 \pm 13$ nm, $D = 7 \pm 1$ nm; (d, h) $L = 174 \pm 19$ nm, $D = 6 \pm 1$ nm. Cobalt diameters: (a) $D = 12 \pm 3$ nm; (b) $D = 19 \pm 4$ nm; (c) $D = 17 \pm 5$ nm; (d) $D = 14 \pm 3$ nm; cobalt oxide diameters: (e) $D = 19 \pm 4$ nm; (f) $D = 22 \pm 5$ nm; (g) $D = 20 \pm 5$ nm; (h) $D = 19 \pm 4$ nm. All scale bars are 100 nm, and a minimum of 100 particles were analyzed to obtain each size distribution.

cobalt-tipped nanorods to form a number of box and short-chain assemblies as a consequence of the dipolar nature of magnetic tips on the ends of these higher aspect ratio nanorods (Figure 3a,c).

Cobalt oxide-tipped nanorods were obtained by the solution oxidation of cobalt-tipped nanorods. CoNP-tipped dumbbell nanorods were dispersed in DCB, heated to 173 °C, and bubbled with O_2 for 24 h to oxidize metallic Co tips. TEM confirmed the dimensional expansion of Co tips into hollow spheres with shells consisting of polycrystalline cobalt oxide (Co_xO_y) phases (15–23 nm) due to the nanoscale Kirkendall effect (Figure 3b,d). This phenomenon resulted from the mismatch in kinetics of Co diffusion out of the nanoparticle (by vacancy exchange) *versus* O_2 diffusion rates into the particle during the oxidation reaction.[57,88–90] We previously observed the colloidal polymerization of our dipolar, polystyrene-coated CoNPs where oxidation resulted in the formation of hollow cobalt oxide nanowires with fusion of nanoparticle repeating units, as a consequence of the nanoscale Kirkendall effect.[57,91] Hence, in this system, oxidation of cobalt-tipped nanorods afforded a core–shell morphology composed of a PtNP core and cobalt oxide shell at the tips of nanorods. For longer nanorods (126 and 174 nm) exposed to identical conditions, laterally attached CoNPs were also oxidized, resulting in the formation of hollow Co_xO_y spheres without PtNP inclusions (Figure 2e–h). In all cases, we observed that the CdSe@CdS nanorods survived the cobalt deposition and oxidation reactions to enable formation of the desired heterostructured product, as confirmed from HRTEM and XRD. In the case of cobalt oxide-tipped nanorods of longer lengths of CdSe@CdS precursors ($L = 156 \pm 20$ nm, $n = 100$), the formation of nanorod networks was observed, where fused cobalt oxide NP tips on nanorods permanently linked nanorods together. The presence of PtNP tips in the majority of nanorods could be imaged in the center of the lower contrast Co_xO_y tips (Figure 3b,d). These fused nanorod assemblies from cobalt oxide NP tip junctions formed as a consequence of the dipolar assembly of CoNP-tipped nanorods, which were captured in solution during oxidation (Figure 3b) as previously observed for dipolar ferromagnetic cobalt nanoparticles.[91] Interestingly, colloidal polymerization of these heterostructured CoNP-tipped nanorods revealed the formation of end-to-end nanorod assemblies, which carried the semiconducting nanorod functionality into the polymerized cobalt oxide network. This phenomenon is among one of the few examples of a creating well-defined p–n junctions, which arise from the precise structure of nanorod colloidal monomers.[30,84,91–97]

High-angle annular dark field scanning transmission electron microscopy (HAADF-STEM) and high-resolution transmission electron microscopy were utilized for structural analysis of the composition of cobalt- and cobalt oxide-tipped heterostructured nanorods. HAADF-STEM (Figure 4) of the nanorod products after the cobalt deposition reaction exhibited a complex core–shell morphology containing a bright core, corresponding to PtNP tips positioned in the center of a lighter contrast shell composed of metallic cobalt with a thin passivation layer of cobalt oxide/hydroxide formed from exposure to air (Figure 4c). HAADF-STEM imaging confirmed the distribution of matchstick and dumbbell PtNP-tipped CdSe@CdS

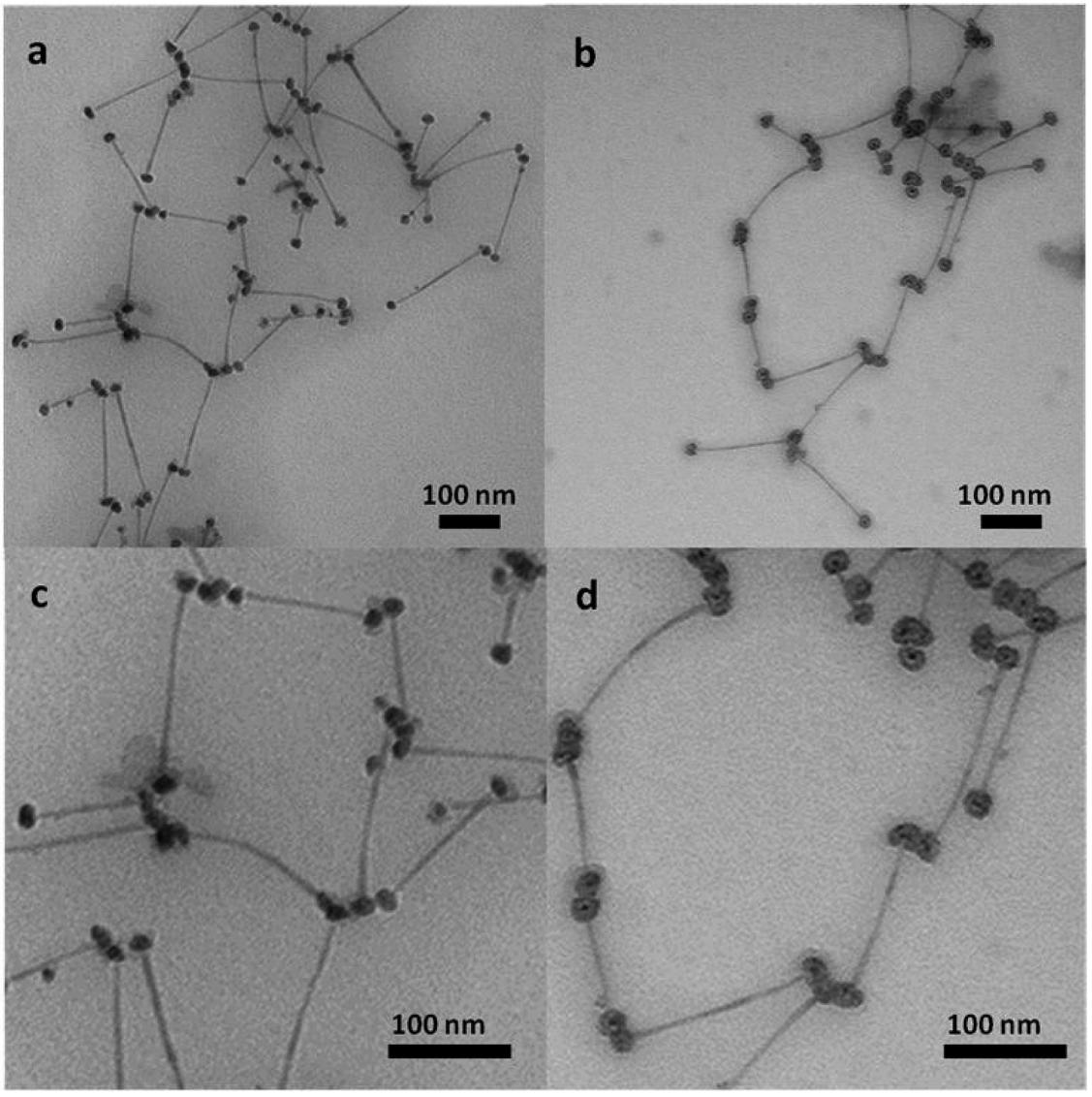

Figure 3. Longer (156 ± 20 nm; *n* = 100) Co-tipped nanorods with little to no lateral Co inclusions before (a, c) and after (b, d) oxidation. Lateral cobalt inclusions were suppressed by reducing the concentration of cobalt precursor in the cobalt-tipping step.

nanorods, as noted by the absence of bright PtNP cores in a fraction of the cobalt-tipped nanorods (Figure 4b).

HRTEM and analysis of the power spectra (PSs, defined as the square of the Fourier transform of the HRTEM image data) of cobalt- and cobalt oxide-tipped nanorods confirmed the connectivity and morphology of the desired product (Figure 5). The presence of intact wurtzite CdS nanorods was proven by the PSs of the regions indicated by the circle in Figure 5, which were characteristic of the wurtzite structure imaged along the [010] zone axis (Figure 5b and d). As expected from previous studies, the long axis of the nanorod was parallel to the wurtzite [001]. It is also important to stress that the CdS nanorods were not affected by the oxidation treatment, as denoted by the similarity of the HRTEM and the PSs of the nanorod regions before and after the reaction. Previous to the oxidation treatment the nanorods were tipped with metallic CoNPs. In the particular example shown in Figure 5a, a CoNP tip was deposited onto a CdSe@CdS nanorod that did not contain a PtNP tip as the seed. The nanorod in Figure 5c was tipped with a polycrystalline shell of rocksalt CoO with a face centered cubic (fcc) core of Pt. The PS from a part of the outer oxidized shell (Figure 5e) showed several reflections with *d*-spacing corresponding to the 111, 200, and 220 of the CoO rocksalt structure. The CoO crystallite size extracted from HRTEM images was found to be smaller than 3 nm. The center of the tip displays higher contrast than the shell, and the PS presents a sharp 111 family of reflections characteristic of the Pt fcc structure (Figure 5f). This PS also shows some diffuse and low-intensity spots attributed to the 111 reflections of CoO, confirming that the polycrystalline CoO shell grew homogeneously around the Pt tip.

Characterization of the intermediates and products of this multistep total synthesis of cobalt oxide-tipped nanorods was also conducted using thermal gravimetric analysis (TGA), vibrating sample magnetometry, optical spectroscopy, and XRD, which confirmed the preparation of the desired dumbbell nanorod product (details are available in the Supporting Information, Sections 2−5, respectively).

Control Experiments. Control experiments were conducted to confirm the need for using Pt-tipped CdSe@CdS nanorods for the deposition of CoNPs with PS-COOH ligands. Attempts to directly deposit CoNP tips onto CdSe@CdS nanorods *via* the thermolysis of $Co_2(CO)_8$ using PS-COOH ligands afforded only nonattached, free CoNPs along with the bare nanorods (Supporting Information Figure S17a,b). Additionally, CoNP deposition experiments using blends of unmodified CdSe@CdS and PtNP-tipped CdSe@CdS nanorods afforded mixtures of bare CdSe@CdS nanorods and two-sided CoNP-tipped nanorods (Supporting Information Figure S17c,d). Furthermore, an entire series of control experiments investigating the effects of key reagents in the PtNP deposition step were conducted and correlated with efficacy of seeding the growth of two-sided CoNPs (see Supporting Information Figures S18−S20). The effect of other experimental parameters in the PtNP deposition step, such as exposure to light and oxygen, was also investigated (see Supporting Information Figure S21).[79,86,98] This series of experiments confirmed the advantages of using PtNP tips on CdSe@CdS nanorods as seeds to promote selective deposition of metallic CoNP tips and confirmed that the thermolysis of $Co_2(CO)_8$ using PS-COOH ligands at $T = 173$ °C in DCB was dramatically altered by growth in the presence of PtNP-tipped CdSe@CdS nanorods.

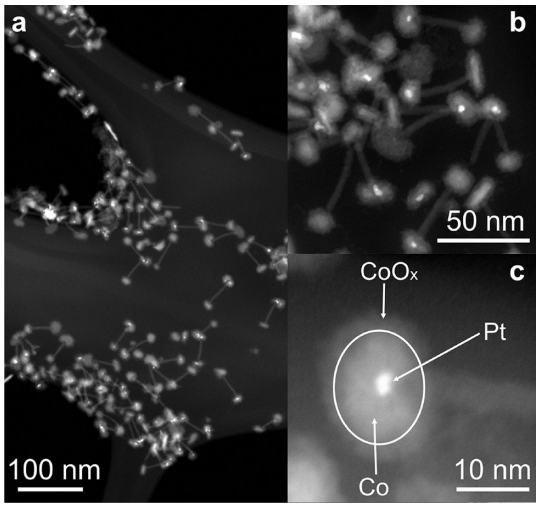

Figure 4. (a−c) HAADF-STEM images of Co-tipped nanorods reveal a distribution of core@shell tips and purely Co tips. Nanorod dimensions: $L = 40 \pm 4$ nm, $D = 6 \pm 1$ nm, $n = 100$; cobalt diameter: $D = 12 \pm 3$ nm, $n = 100$.

Kinetic Investigations into Pt-Deposition Reactions and Correlation with CoNP-Tipping Topology. While the synthetic methodology described in previous sections enabled efficient synthesis of CoNP- and CoONP-tipped nanorods, a number of synthetic and mechanistic questions arose that warranted deeper investigation. It is known that metal-tipped matchstick II−VI semiconductor nanorods (*e.g.*, CdSe, CdS, CdSe@CdS) are accessible due to preferential deposition of metals onto chalcogen (*e.g.*, Se, S)-rich facets of semiconductor nanorod termini.[64,66,74,79] However, enhanced ligand coverage of the metal-rich (Cd-rich) facets at the diametrically opposed ends of chalcogenide nanorods was observed to inhibit metal deposition.[99] Consequently, the symmetric deposition of metal NP tips of identical particle size is significantly more challenging, as evidenced by the limited number of systems that have been developed.[66,68,74] Since control experiments

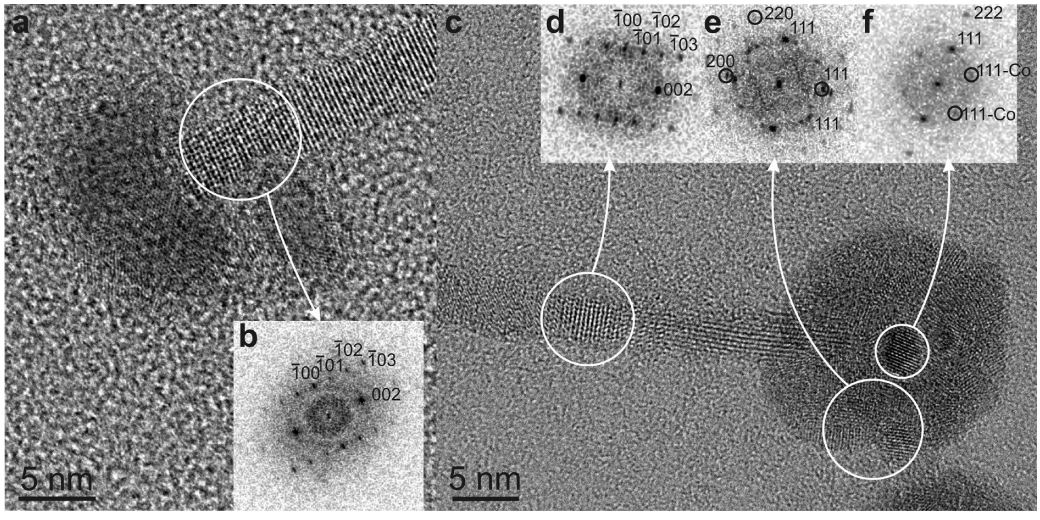

Figure 5. HRTEM and power spectrum analysis used to determine the crystalline phases in (core@shell) (a, b) Pt@Co-tipped and (c−f) Pt@CoO-tipped nanorods. Nanorod dimensions: $L = 40 \pm 4$ nm, $D = 6 \pm 1$ nm, $n = 100$; cobalt diameter: $D = 12 \pm 3$ nm, $n = 100$.

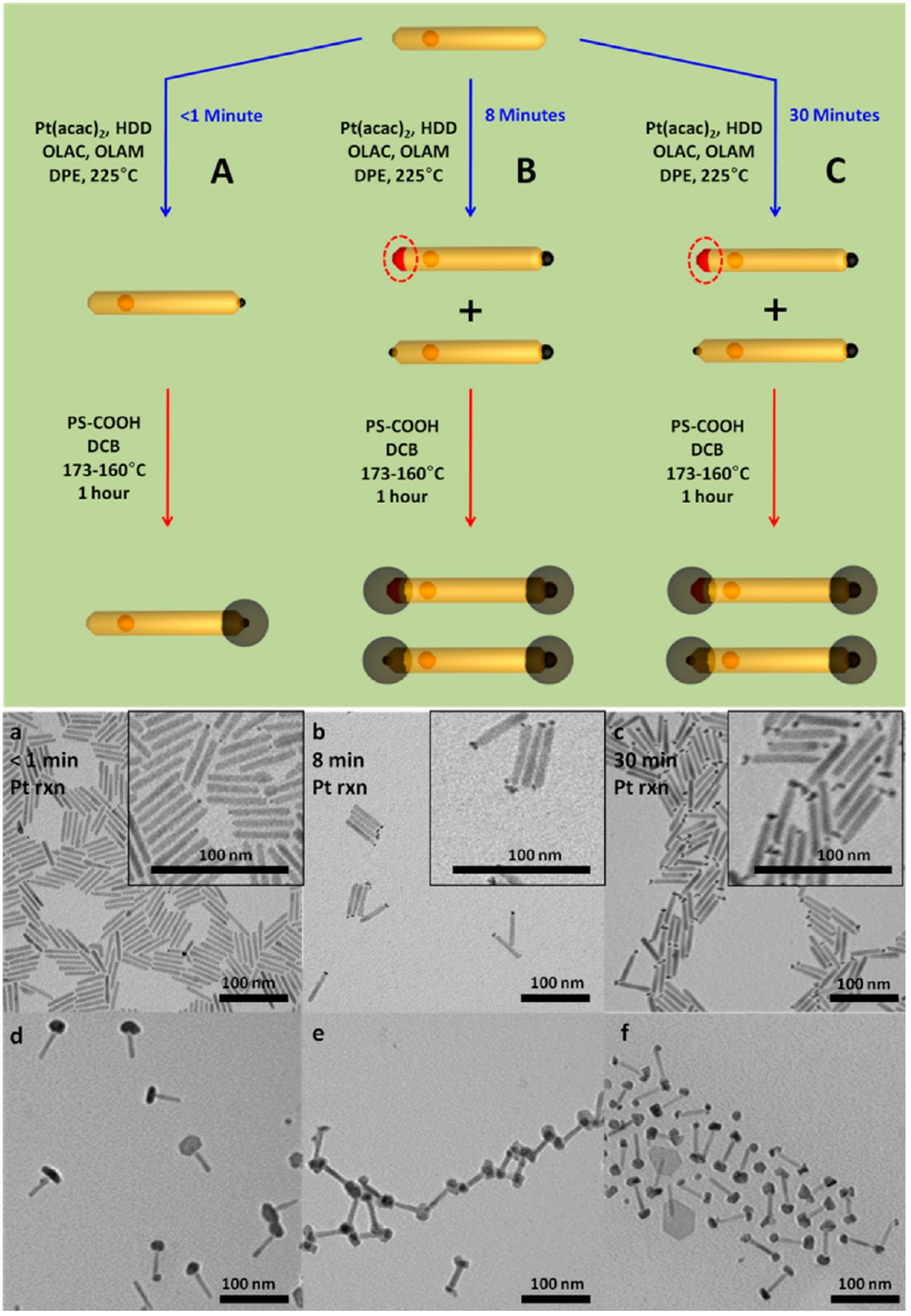

Figure 6. Temporal resolution of "unactivated" matchstick PtNP-tipped nanorods from "activated" matchstick PtNP-tipped rods. (A–C) Reaction schemes for products shown by TEM below. (A) Allowing the platinum-tipping reaction to run for up to 1 min results in primarily matchstick PtNP-tipped nanorods and free nanorods. Treating this mixture with Co precursors results in matchstick CoNP-tipped products and free nanorods. (B, C) Longer Pt-tipping reaction times result in mixtures of PtNP-tipped products that are subsequently dumbbell CoNP-tipped. (a–c) Products of the platinum-tipping reaction after (a) 45 s, (b) 8 min (normal reaction time), and (c) 30 min. (d–f) Products of cobalt-tipping the above platinum-tipped products: (d) primarily matchstick Co-tipped; (e, f) primarily dumbbell Co-tipped. All scale bars are 100 nm.

confirmed that unmodified CdSe@CdS nanorods were unable to seed the growth of CoNP tips, the synthetic parameters central to the PtNP-tip formation were revisited. The initial hypothesis that two-sided

PtNP-tipped CdSe@CdS nanorods would be required to form two-sided CoNP-tipped nanorod dumbbells was inconsistent with the experimental finding that the as-synthesized mixture of matchstick and dumbbell Pt-tipped CdSe@CdS nanorods afforded high yields of two-sided CoNP-tipped dumbbell nanorods. The remaining question of interest was the nature of apparently *one-sided* PtNP-tipped CdSe@CdS matchstick nanorods that promoted *two-sided* deposition of CoNP tips onto nanorods.

To interrogate these mechanistic questions, a kinetic investigation of the PtNP deposition reaction onto CdSe@CdS nanorods (L = 43 + 4 nm; D = 5 + 1 nm) was conducted to ascertain if the formation of one-sided Pt-tipped matchstick nanorods could be temporally resolved from two-sided Pt-tipped dumbbell nanorods. After very short reaction times (1 min), a mixture of bare CdSe@CdS nanorods (approximately 20%) and one-sided Pt-tipped CdSe@CdS matchstick nanorods (approximately 70%) was observed, where the size of PtNP tips were found to be 2−3 nm from TEM. At longer reaction times, PtNP-tip growth was statistically accompanied by PtNP deposition onto the opposing nanorod terminus. Longer reaction times resulted in the growth of existing PtNP tips and formation of additional PtNP tips per nanorod on average. In the case of nanorods with two PtNPs attached to the same terminus, longer reaction times resulted in the coalescence of the individual PtNP tips into larger, irregularly shaped PtNP tips. The morphology of these resulting asymmetrically tipped structures was observed by TEM (similar to Figure 1d,e) after reaction times of 8 min. TEM of reaction mixture aliquots indicated the populations of bare CdSe@CdS nanorods, one-sided PtNP-tipped nanorods, and two-sided PtNP-tipped nanorods were observed to plateau after 8 min, which over a small population of 141 nanorods afforded ratios of 4:66:30, respectively. Longer reaction times (30 min) did not afford a higher yield of two-sided Pt-tipped nanorods, where the ratio of bare nanorods to one- and two-sided PtNP nanorods remained essentially unchanged (see Figure 6b,c and Supporting Information Figure S23).

CoNP deposition experiments were then conducted for three different Pt-tipped nanorods that were quenched at varying reaction times (<1, 8, and 30 min) during the PtNP-tipping reaction in order to correlate Pt-tip morphology with topology of CoNP tips. For Pt-tipped nanorods quenched after less than 1 min (approximately 45 s) and then subjected to CoNP deposition chemistry, TEM revealed that the majority of the product (>50%) was one-sided CoNP-tipped matchstick nanorods with a small fraction of some (<10%) two-sided CoNP-tipped dumbbell nanorods (Figure 6a,d). Conversely, almost exclusive formation of two-sided CoNP-tipped nanorods (90%) occurred when the mixture of one- and two-sided Pt-tipped

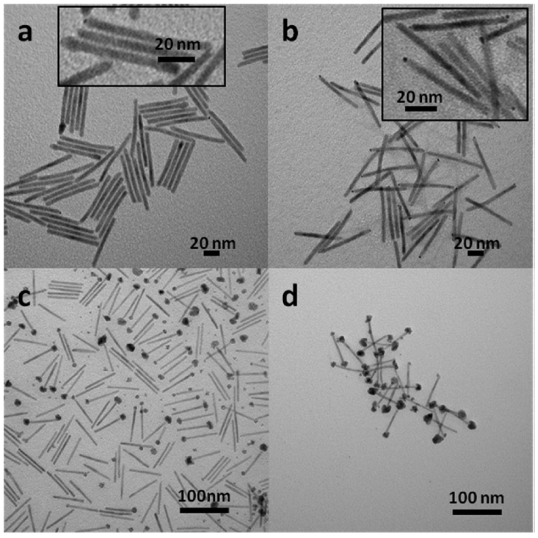

Figure 7. (a) Isolated matchstick Pt-tipped and unmodified nanorods after 20 s reaction time. (b) Mixture of matchstick and dumbbell Pt-tipped nanorods after Pt-tipping the products from part a for 45 s. Insets in parts a and b show the small PtNP tips in these samples. (c) Mixture of unmodified and matchstick Co-tipped products from treating Pt-tipped nanorods from part a with Co-tipping conditions. (d) Primarily dumbbell Co-tipped products from treating part b with Co-tipping conditions.

CdSe@CdS nanorod precursors (formed after reaction times of 8 and 30 min) was subjected to CoNP deposition chemistry with very small fractions of one-sided CoNP-tipped matchstick nanorods (4%) (Figure 6b,e and 6c,f, respectively). These kinetic experiments revealed that the synthesis of one-sided PtNP-tipped matchstick nanorods could be kinetically controlled, which further afforded the synthesis of one-sided CoNP-tipped matchstick nanorods (along with some unreacted bare CdSe@CdS nanorods). Hence, by quenching PtNP reactions to very short reaction time (<1 min), selective activation of only one nanorod terminus was achieved. However, at longer reaction times in the Pt-deposition reaction (8 and 30 min), these untipped nanorod ends were also chemically activated for CoNP deposition, without any visually detectable changes in the nanorod morphology as revealed by TEM imaging.

A critical set of experiments were conducted where nanorod precursors that afforded one-sided CoNP-tipped nanorods were activated by an additional chemical treatment to primarily afford two-sided CoNP-tipped nanorods. One-sided Pt-tipped nanorods (PtNP tip size <3 nm) were initially synthesized that were quenched after very short reaction time (<1 min) and were confirmed to primarily afford one-sided CoNP-tipped nanorods upon treatment with PS-COOH and $Co_2(CO)_8$, as previously described (Figure 7a,c). These same one-sided Pt-tipped nanorods (same batch, different experiments) were subjected to an additional PtNP deposition step, by exposure to $Pt(acac)_2$, oleylamine, oleic acid, and 1,2-hexadecanediol at elevated

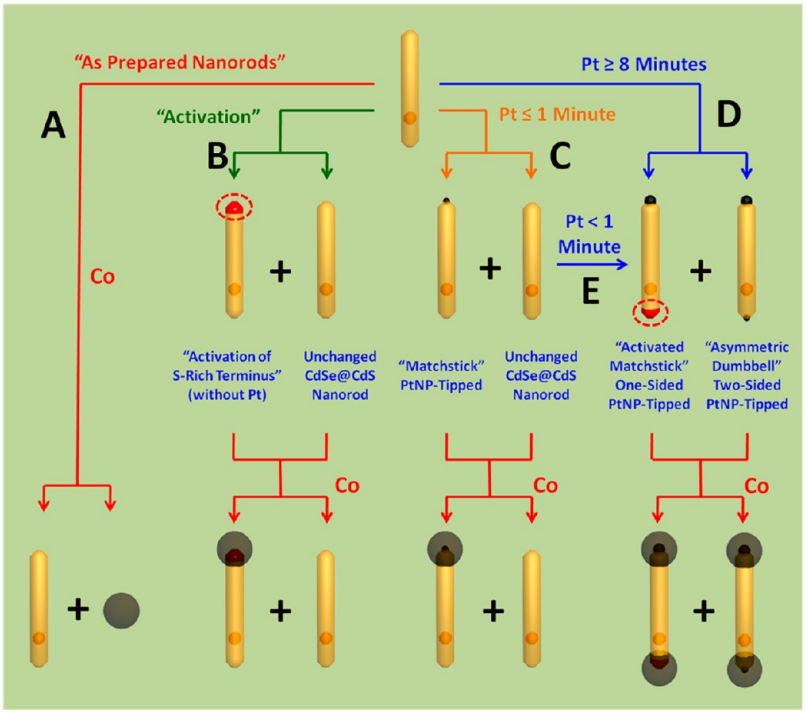

Scheme 2. Cartoon summarizing the options presented in this work: (A) Directly Co-tipping unmodified nanorods results in no reaction between Co and parent nanorods. Free CoNPs and parent nanorods are formed. (B) "Activation" of the parent nanorods by etching in the absence of Pt precursors results in activation of one terminus only toward Co-tipping. The products of this reaction are matchstick CoNP-tipped and unmodified nanorods, where dashed circles indicate an "activated" terminus. (C) Kinetic resolution of "true matchsticks": Treating with Pt-tipping conditions for 1 min or less gives a mixture of matchstick PtNP-tipped nanorods and unchanged nanorods, which subsequently provide matchstick CoNP-tipped nanorods. (D) Allowing the Pt-tipping reaction to proceed for 8 min or longer results in a mixture of activated matchstick and dumbbell PtNP-tipped products. This mixture always results in primarily (>90%) dumbbell CoNP-tipped nanorods after treating with Co precursors. (E) Unactivated ("true") Pt-tipped matchsticks can be subsequently activated by further Pt-tipping to provide a mixture of activated Pt-tipped matchsticks and dumbbells with similar reactivity to those from route D.

temperature. TEM confirmed that a higher yield of two-sided PtNP-tipped nanorods was obtained after this second PtNP deposition step, where PtNP tip sizes were still much smaller (less than 3 nm) than in conditions previously described (Figure 7b). However, it is important to note that approximately 50% of these products were still one-sided Pt-tipped matchstick nanorods. CoNP deposition onto these mixtures of one- and two-sided PtNP-tipped nanorods almost exclusively formed two-sided CoNP-tipped nanorods in a fashion similar to those obtained for earlier one-pot activation conditions described previously (Figure 7d). These experiments revealed that the yield of both matchstick and dumbbell CoNP-tipped nanorods could be kinetically controlled using purely chemical methods to control the preparation of PtNP- and CoNP-tipped nanorods. It can be further concluded that electronic coupling within the heterostructured nanorod or electrochemical mechanisms was not at work in the selective formation of two-sided CoNP-tipped dumbbell nanorods under these reaction conditions.

To investigate the contribution of chemical etching on the activation of nanorods for CoNP deposition, a series of control experiments were conducted by systematic treatment of rods with the reagents used in the PtNP deposition reaction. Native CdSe@CdS nanorods ($L = 45 \pm 4$ nm, $D = 7 \pm 1$ nm) were treated with oleic acid, oleylamine, and 1,2-hexadecanediol in diphenyl ether at 225 °C for 8 min and subjected to CoNP deposition reactions to afford a mixture of one-sided CoNP-tipped matchstick nanorods (CoNP tip diameter (D) = 17 ± 3 nm) and bare CdSe@CdS nanorods, with a minimal yield of two-sided CoNP-tipped dumbbell nanorods (Supporting Information Figure S18). The overall yield of CoNP-tipped matchstick nanorods was significantly lower in contrast to experiments using Pt-tipped nanorod precursors. CoNP-tipped nanorods prepared by chemical activation of bare CdSe@CdS nanorods also exhibited a more random placement of CoNPs along the nanorod, in contrast to selective deposition onto nanorod termini. Nevertheless, this experiment revealed that the mixture of ligands and reducing agent used in the Pt deposition step was sufficient to chemically activate one terminus of the CdSe@CdS nanorod to enable one-sided deposition of a single CoNP tip.

The kinetic and morphological observations presented above are consistent with previous reports correlating structure and reactivity of wurtzite chalcogenide nanorods, where the chalcogen-rich $\{00\bar{1}\}$

facet was found to be more reactive toward metal deposition than the diametrically opposed cadmium-rich {001} facet for wurtzite CdSe@CdS and CdS nanorods.[64,66,74,79,86,100] In the present report, PtNP-tip deposition was observed to occur preferentially at one terminus for a given nanorod followed by statistical growth of a second, smaller, PtNP tip at the diametrically opposed nanorod terminus after additional reaction time. The second, smaller, PtNP tip was generally observed to be deposited off-center with respect to the long axis of the nanorod substrate (Figure 1,Figure 6, and Supporting Information Figure S22). We assign the sulfur-rich $\{00\bar{1}\}$ facet as the location of initial PtNP-tip deposition onto CdSe@CdS nanorods due to its known greater chemical availability and reactivity toward metal deposition.[64,79,86,99−101] The diametrically opposed nanorod terminus can be assigned to the {001} Cd-rich end of the wurtzite CdS nanorod phase, where metal growth has been observed to preferentially proceed onto diagonally positioned sulfur-rich $\{10\bar{1}\}$ facets as previously reported by Ryan *et al*. and Banin *et al*.[86,100] HRTEM attempts to directly image CdSe seeds imbedded in CdSe@CdS nanorods in this report were unsuccessful, presumably due to the smaller (<2.8 nm) CdSe seed sizes used to grow CdSe@CdS nanorods with diameters averaging 5−7 nm, in contrast to related reports.[28,64]

We were unable to eliminate the possibility that "activated" PtNP-tipped matchsticks have a trace amount of platinum present on the {001} Cd-rich facet (or sulfur-rich $\{10\bar{1}\}$ facet), which is sufficient to promote Co deposition, but below the detection limits of TEM. Simple calculations show that samples containing >60% apparently one-sided matchstick PtNP-tipped nanorods by TEM would need a small, undetectable, amount of platinum on >83% of the apparent PtNP-tipped "matchsticks" to reach the observed Co-tipped product distributions (>90% CoNP-tipped dumbbells).

SYNTHETIC CHALLENGES

We found that several unorthodox techniques and previously unpublished considerations were required in reproducing and scaling up the colloidal syntheses in this work. As these are infrequently mentioned in the literature, we would like to notify the reader that we have included all pertinent details in the Supporting Information including centrifuge rotor diameter, quantum dot synthesis quenching, insulation of the reaction vessel for synthesis of nanorods, sensitivity to sonication, methods for obtaining yields from colloidal dispersions, and calculations used for molecular weights of colloids. While some of these items have been reported individually in other publications, we offer a collection herein.

CONCLUSION

Methods to selectively synthesize CoNP- and Co_xO_yNP-tipped CdSe@CdS nanorods with controlled matchstick or dumbbell morphologies were established *via* a five-step total synthesis. The morphology and connectivity of CoNP tips were shown to evolve as a direct consequence of the conditions used to obtain PtNP-tipped nanorod precursors, which gave mixtures of matchstick and dumbbell PtNP-tipped morphologies. These precursors were found to drive nearly quantitative CoNP-tipped dumbbell formation due to either chemical activation of the untipped terminus or trace amounts of platinum at the apparently untipped terminus of PtNP-tipped matchsticks. This synthetic methodology, along with detailed synthetic procedures, offers an alternative strategy to prepare heterostructured nanorods with core−shell nanoparticle tips that enable the creation of nanoscopic semiconductor or Schottky-type junctions. Future efforts will examine the electronic structure and photoelectrochemistry of these nanocomposite materials.

METHODS

Details on the synthesis and characterization of nanorod precursors, intermediates, and products are discussed in the Supporting Information.

Conflict of Interest: The authors declare no competing financial interest.

Acknowledgment. This work was funded by the Division of Chemical Science, Geosciences and Biosciences, Office of Basic Energy Sciences of the U.S. Department of Energy (DE-FG03-02ER15753) (L.J.H., J.P.), the NSF CAREER Program (DMR-0645618) (M.M.B., N.E.R., D.G., J.P.), the World Class University Program through the National Research Foundation of Korea funded by the Ministry of Education, Science and Technology (R31-10013) (Y.S.), and the Alfred P. Sloan Foundation (P.T.D., J. P.) are acknowledged for synthetic support of this work. K.C. acknowledges financial support from NRF for the National Creative Research Initiative Center for Intelligent Hybrids (2010-0018290).

Supporting Information Available: TEM images for control experiments and synthesized intermediates, synthetic details for each step, characterization (optical, XRD, magnetic, TGA), and trends are available free of charge *via* the Internet at http://pubs.acs.org.

REFERENCES AND NOTES

1. Costi, R.; Saunders, A. E.; Banin, U. Colloidal Hybrid Nanostructures: A New Type of Functional Materials. *Angew. Chem., Int. Ed.* **2010**, *49*, 4878–4897.
2. Wang, C.; Xu, C. J.; Zeng, H.; Sun, S. H. Recent Progress in Syntheses and Applications of Dumbbell-Like Nanoparticles. *Adv. Mater.* **2009**, *21*, 3045–3052.

3. Cozzoli, P. D.; Pellegrino, T.; Manna, L. Synthesis, Properties and Perspectives of Hybrid Nanocrystal Structures. *Chem. Soc. Rev.* **2006**, *35*, 1195–1208.
4. Amirav, L.; Alivisatos, A. P. Photocatalytic Hydrogen Production with Tunable Nanorod Heterostructures. *J. Phys. Chem. Lett.* **2010**, *1*, 1051–1054.
5. Khan, M. A.; Yang, O. B. Photocatalytic Water Splitting for Hydrogen Production under Visible Light on Ir and Co Ionized Titania Nanotube. *Catal. Today* **2009**, *146*, 177–182.
6. Maeda, K.; Domen, K. New Non-Oxide Photocatalysts Designed for Overall Water Splitting under Visible Light. *J. Phys. Chem. C* **2007**, *111*, 7851–7861.
7. Costi, R.; Saunders, A. E.; Elmalem, E.; Salant, A.; Banin, U. Visible Light-Induced Charge Retention and Photocatalysis with Hybrid CdSe-Au Nanodumbbells. *Nano Lett.* **2008**, *8*, 637–641.
8. Sudeep, P. K.; Takechi, K.; Kamat, P. V. Harvesting Photons in the Infrared. Electron Injection from Excited Tricarbocyanine Dye (IR-125) into TiO_2 and Ag@TiO_2 Core–Shell Nanoparticles. *J. Phys. Chem. C* **2006**, *111*, 488–494.
9. Hirakawa, T.; Kamat, P. V. Photoinduced Electron Storage and Surface Plasmon Modulation in Ag@TiO2 Clusters. *Langmuir* **2004**, *20*, 5645–5647.
10. Maeda, K.; Sakamoto, N.; Ikeda, T.; Ohtsuka, H.; Xiong, A.; Lu, D.; Kanehara, M.; Teranishi, T.; Domen, K. Preparation of Core–Shell-Structured Nanoparticles (with a Noble-Metal or Metal Oxide Core and a Chromia Shell) and Their Application in Water Splitting by Means of Visible Light. *Chem.—Eur. J.* **2010**, *16*, 7750–7759.
11. Maeda, K.; Xiong, A.; Yoshinaga, T.; Ikeda, T.; Sakamoto, N.; Hisatomi, T.; Takashima, M.; Lu, D.; Kanehara, M.; Setoyama, T.; *et al*. Photocatalytic Overall Water Splitting Promoted by Two Different Cocatalysts for Hydrogen and Oxygen Evolution under Visible Light. *Angew. Chem., Int. Ed.* **2010**, *49*, 4096–4099.
12. Bao, N.; Shen, L.; Takata, T.; Domen, K. Self-Templated Synthesis of Nanoporous CdS Nanostructures for Highly Efficient Photocatalytic Hydrogen Production under Visible Light. *Chem. Mater.* **2007**, *20*, 110–117.
13. Lewis, N. S.; Nocera, D. G. Powering the Planet: Chemical Challenges in Solar Energy Utilization. *Proc. Natl. Acad. Sci. U. S. A.* **2006**, *103*, 15729–15735.
14. Mills, A.; Davies, R. H.; Worsley, D. Water Purification by Semiconductor Photocatalysis. *Chem. Soc. Rev.* **1993**, *22*, 417–425.
15. Wood, A.; Giersig, M.; Mulvaney, P. Fermi Level Equilibration in Quantum Dot–Metal Nanojunctions. *J. Phys. Chem. B* **2001**, *105*, 8810–8815.
16. Govorov, A. O.; Bryant, G. W.; Zhang, W.; Skeini, T.; Lee, J.; Kotov, N. A.; Slocik, J. M.; Naik, R. R. Exciton–Plasmon Interaction and Hybrid Excitons in Semiconductor–Metal Nanoparticle Assemblies. *Nano Lett.* **2006**, *6*, 984–994.
17. Tang, M. L.; Grauer, D. C.; Lassalle-Kaiser, B.; Yachandra, V. K.; Amirav, L.; Long, J. R.; Yano, J.; Alivisatos, A. P. Structural and Electronic Study of an Amorphous MoS_3 Hydrogen-Generation Catalyst on a Quantum-Controlled Photosensitizer. *Angew. Chem., Int. Ed.* **2011**, *50*, 10203–10207.
18. Kumar, S.; Jones, M.; Lo, S. S.; Scholes, G. D. Nanorod Heterostructures Showing Photoinduced Charge Separation. *Small* **2007**, *3*, 1633–1639.
19. Shemesh, Y.; Macdonald, J. E.; Menagen, G.; Banin, U. Synthesis and Photocatalytic Properties of a Family of CdS-PdX Hybrid Nanoparticles. *Angew. Chem., Int. Ed.* **2011**, *50*, 1185–1189.
20. Elmalem, E.; Saunders, A. E.; Costi, R.; Salant, A.; Banin, U. Growth of Photocatalytic CdSe–Pt Nanorods and Nanonets. *Adv. Mater.* **2008**, *20*, 4312–4317.
21. Pacholski, C.; Kornowski, A.; Weller, H. Site-Specific Photodeposition of Silver on ZnO Nanorods. *Angew. Chem., Int. Ed.* **2004**, *43*, 4774–4777.
22. Saruyama, M.; So, Y.-G.; Kimoto, K.; Taguchi, S.; Kanemitsu, Y.; Teranishi, T. Spontaneous Formation of Wurzite-CdS/Zinc Blende-CdTe Heterodimers through a Partial Anion Exchange Reaction. *J. Am. Chem. Soc.* **2011**, *133*, 17598–17601.
23. Steiner, D.; Mokari, T.; Banin, U.; Millo, O. Electronic Structure of Metal-Semiconductor Nanojunctions in Gold CdSe Nanodumbbells. *Phys. Rev. Lett.* **2005**, *95*, 056805–1.
24. Talapin, D. V.; Koeppe, R.; Gotzinger, S.; Kornowski, A.; Lupton, J. M.; Rogach, A. L.; Benson, O.; Feldmann, J.; Weller, H. Highly Emissive Colloidal CdSe/CdS Heterostructures of Mixed Dimensionality. *Nano Lett.* **2003**, *3*, 1677–1681.
25. Milliron, D. J.; Hughes, S. M.; Cui, Y.; Manna, L.; Li, J.; Wang, L.-W.; Paul Alivisatos, A. Colloidal Nanocrystal Heterostructures with Linear and Branched Topology. *Nature* **2004**, *430*, 190–195.
26. Shieh, F.; Saunders, A. E.; Korgel, B. A. General Shape Control of Colloidal CdS, CdSe, CdTe Quantum Rods and Quantum Rod Heterostructures. *J. Phys. Chem. B* **2005**, *109*, 8538–8542.
27. Kumar, S.; Nann, T. Shape Control of II-VI Semiconductor Nanomateriats. *Small* **2006**, *2*, 316–329.
28. Carbone, L.; Nobile, C.; De Giorgi, M.; Sala, F. D.; Morello, G.; Pompa, P.; Hytch, M.; Snoeck, E.; Fiore, A.; Franchini, I. R.; *et al*. Synthesis and Micrometer-Scale Assembly of Colloidal CdSe/CdS Nanorods Prepared by a Seeded Growth Approach. *Nano Lett.* **2007**, *7*, 2942–2950.
29. Talapin, D. V.; Nelson, J. H.; Shevchenko, E. V.; Aloni, S.; Sadtler, B.; Alivisatos, A. P. Seeded Growth of Highly Luminescent CdSe/CdS Nanoheterostructures with Rod and Tetrapod Morphologies. *Nano Lett.* **2007**, *7*, 2951–2959.
30. Talapin, D. V.; Yu, H.; Shevchenko, E. V.; Lobo, A.; Murray, C. B. Synthesis of Colloidal PbSe/PbS Core-Shell Nanowires and PbS/Au Nanowire-Nanocrystal Heterostructures. *J. Phys. Chem. C* **2007**, *111*, 14049–14054.
31. Dorfs, D.; Salant, A.; Popov, I.; Banin, U. ZnSe Quantum Dots within CdS Nanorods: A Seeded-Growth Type-II System. *Small* **2008**, *4*, 1319–1323.
32. Reiss, P.; Protiere, M.; Li, L. Core/Shell Semiconductor Nanocrystals. *Small* **2009**, *5*, 154–168.
33. Sitt, A.; Salant, A.; Menagen, G.; Banin, U. Highly Emissive Nano Rod-in-Rod Heterostructures with Strong Linear Polarization. *Nano Lett.* **2011**, *11*, 2054–2060.
34. Mokari, T.; Banin, U. Synthesis and Properties of CdSe/ZnS Core/Shell Nanorods. *Chem. Mater.* **2003**, *15*, 3955–3960.
35. Jun, Y. W.; Jung, Y. Y.; Cheon, J. Architectural Control of Magnetic Semiconductor Nanocrystals. *J. Am. Chem. Soc.* **2002**, *124*, 615–619.
36. Yong, K. T.; Sahoo, Y.; Swihart, M. T.; Prasad, P. N. Growth of CdSe Quantum Rods and Multipods Seeded by Noble-Metal Nanoparticles. *Adv. Mater.* **2006**, *18*, 1978–1982.
37. Shi, W.; Sahoo, Y.; Zeng, H.; Ding, Y.; Swihart, M. T.; Prasad, P. N. Anisotropic Growth of PbSe Nanocrystals on Au–Fe_3O_4 Hybrid Nanoparticles. *Adv. Mater.* **2006**, *18*, 1889–1894.
38. Piao, Y.; Kim, J.; Na, H. B.; Kim, D.; Baek, J. S.; Ko, M. K.; Lee, J. H.; Shokouhimehr, M.; Hyeon, T. Wrap-Bake-Peel Process for Nanostructural Transformation from [beta]-FeOOH Nanorods to Biocompatible Iron Oxide Nanocapsules. *Nat. Mater.* **2008**, *7*, 242–247.
39. Choi, S.-H.; Kim, E.-G.; Hyeon, T. One-Pot Synthesis of Copper–Indium Sulfide Nanocrystal Heterostructures with Acorn, Bottle, and Larva Shapes. *J. Am. Chem. Soc.* **2006**, *128*, 2520–2521.
40. Choi, S.-H.; Na, H. B.; Park, Y. I.; An, K.; Kwon, S. G.; Jang, Y.; Park, M.-h.; Moon, J.; Son, J. S.; Song, I. C.; *et al*. Simple and Generalized Synthesis of Oxide–Metal Heterostructured Nanoparticles and their Applications in Multimodal Biomedical Probes. *J. Am. Chem. Soc.* **2008**, *130*, 15573–15580.

41. Xing, S. X.; Feng, Y. H.; Tay, Y. Y.; Chen, T.; Xu, J.; Pan, M.; He, J. T.; Hng, H. H.; Yan, Q. Y.; Chen, H. Y. Reducing the Symmetry of Bimetallic Au@Ag Nanoparticles by Exploiting Eccentric Polymer Shells. *J. Am. Chem. Soc.* **2010**, *132*, 9537–9539.
42. Chen, T.; Chen, G.; Xing, S. X.; Wu, T.; Chen, H. Y. Scalable Routes to Janus Au-SiO(2) and Ternary Ag-Au-SiO(2) Nanoparticles. *Chem. Mater.* **2010**, *22*, 3826–3828.
43. Gu, H. W.; Zheng, R. K.; Zhang, X. X.; Xu, B. Facile One-Pot Synthesis of Bifunctional Heterodimers of Nanoparticles: A Conjugate of Quantum Dot and Magnetic Nanoparticles. *J. Am. Chem. Soc.* **2004**, *126*, 5664–5665.
44. Mokari, T.; Aharoni, A.; Popov, I.; Banin, U. Diffusion of Gold into InAs Nanocrystals. *Angew. Chem., Int. Ed.* **2006**, *45*, 8001–8005.
45. Yu, H.; Chen, M.; Rice, P. M.; Wang, S. X.; White, R. L.; Sun, S. H. Dumbbell-Like Bifunctional Au-Fe_3O_4 Nanoparticles. *Nano Lett.* **2005**, *5*, 379–382.
46. Kwon, K.-W.; Shim, M. γ-Fe_2O_3/II−VI Sulfide Nanocrystal Heterojunctions. *J. Am. Chem. Soc.* **2005**, *127*, 10269–10275.
47. Shi, W.; Zeng, H.; Sahoo, Y.; Ohulchanskyy, T. Y.; Ding, Y.; Wang, Z. L.; Swihart, M.; Prasad, P. N. A General Approach to Binary and Ternary Hybrid Nanocrystals. *Nano Lett.* **2006**, *6*, 875–881.
48. Choi, J. S.; Jun, Y. W.; Yeon, S. I.; Kim, H. C.; Shin, J. S.; Cheon, J. Biocompatible Heterostructured Nanoparticles for Multimodal Biological Detection. *J. Am. Chem. Soc.* **2006**, *128*, 15982–15983.
49. Yang, J.; Elim, H. I.; Zhang, Q. B.; Lee, J. Y.; Ji, W. Rational Synthesis, Self-Assembly, and Optical Properties of PbS-Au Heterogeneous Nanostructures *via* Preferential Deposition. *J. Am. Chem. Soc.* **2006**, *128*, 11921–11926.
50. Yang, J.; Levina, L.; Sargent, E. H.; Kelley, S. O. Heterogeneous Deposition of Noble Metals on Semiconductor Nanoparticles in Organic or Aqueous Solvents. *J. Mater. Chem.* **2006**, *16*, 4025–4028.
51. Gu, H.; Yang, Z.; Gao, J.; Chang, C. K.; Xu, B. Heterodimers of Nanoparticles: Formation at a Liquid−Liquid Interface and Particle-Specific Surface Modification by Functional Molecules. *J. Am. Chem. Soc.* **2004**, *127*, 34–35.
52. Buck, M. R.; Bondi, J. F.; Schaak, R. E. A Total-Synthesis Framework for the Construction of High-Order Colloidal Hybrid Nanoparticles. *Nat. Chem.* **2012**, *4*, 37–44.
53. Liz-Marzan, L. M.; Giersig, M.; Mulvaney, P. Synthesis of Nanosized Gold-Silica Core-Sshell Particles. *Langmuir* **1996**, *12*, 4329–4335.
54. Gao, J. H.; Zhang, B.; Gao, Y.; Pan, Y.; Zhang, X. X.; Xu, B. Fluorescent Magnetic Nanocrystals by Sequential Addition of Reagents in a One-Pot Reaction: A Simple Preparation for Multifunctional Nanostructures. *J. Am. Chem. Soc.* **2007**, *129*, 11928–11935.
55. Kim, H.; Achermann, M.; Balet, L. P.; Hollingsworth, J. A.; Klimov, V. I. Synthesis and Characterization of Co/CdSe Core/Shell Nanocomposites: Bifunctional Magnetic-Optical Nanocrystals. *J. Am. Chem. Soc.* **2004**, *127*, 544–546.
56. Lin, H. Y.; Chen, Y. F.; Wu, J. G.; Wang, D. I.; Chen, C. C. Carrier Transfer Induced Photoluminescence Change in Metal-Semiconductor Core-Shell Nanostructures. *Appl. Phys. Lett.* **2006**, *88*, 161911.
57. Yin, Y. D.; Rioux, R. M.; Erdonmez, C. K.; Hughes, S.; Somorjai, G. A.; Alivisatos, A. P. Formation of Hollow Nanocrystals through the Nanoscale Kirkendall Effect. *Science* **2004**, *304*, 711–714.
58. Peng, X.; Schlamp, M. C.; Kadavanich, A. V.; Alivisatos, A. P. Epitaxial Growth of Highly Luminescent CdSe/CdS Core/Shell Nanocrystals with Photostability and Electronic Accessibility. *J. Am. Chem. Soc.* **1997**, *119*, 7019–7029.
59. Tan, L. H.; Xing, S. X.; Chen, T.; Chen, G.; Huang, X.; Zhang, H.; Chen, H. Y. Fabrication of Polymer Nanocavities with Tailored Openings. *ACS Nano* **2009**, *3*, 3469–3474.
60. Liu, M. Z.; Guyot-Sionnest, P. Preparation and Optical Properties of Silver Chalcogenide Coated Gold Nanorods. *J. Mater. Chem.* **2006**, *16*, 3942–3945.
61. Lee, J.; Javed, T.; Skeini, T.; Govorov, A. O.; Bryant, G. W.; Kotov, N. A. Bioconjugated Ag Nanoparticles and CdTe Nanowires: Metamaterials with Field-Enhanced Light Absorption. *Angew. Chem., Int. Ed.* **2006**, *45*, 4819–4823.
62. Lee, J.; Govorov, A. O.; Dulka, J.; Kotov, N. A. Bioconjugates of CdTe Nanowires and Au Nanoparticles: Plasmon−Exciton Interactions, Luminescence Enhancement, and Collective Effects. *Nano Lett.* **2004**, *4*, 2323–2330.
63. Casavola, M.; Grillo, V.; Carlino, E.; Giannini, C.; Gozzo, F.; Pinel, E. F.; Garcia, M. A.; Manna, L.; Cingolani, R.; Cozzoli, P. D. Topologically Controlled Growth of Magnetic-Metal-Functionalized Semiconductor Oxide Nanorods. *Nano Lett.* **2007**, *7*, 1386–1395.
64. Deka, S.; Falqui, A.; Bertoni, G.; Sangregorio, C.; Poneti, G.; Morello, G.; De Giorgi, M.; Giannini, C.; Cingolani, R.; Manna, L.; *et al.* Fluorescent Asymmetrically Cobalt-Tipped CdSe@CdS Core@Shell Nanorod Heterostructures Exhibiting Room-Temperature Ferromagnetic Behavior. *J. Am. Chem. Soc.* **2009**, *131*, 12817–12828.
65. Buonsanti, R.; Grillo, V.; Carlino, E.; Giannini, C.; Gozzo, F.; Garcia-Hernandez, M.; Garcia, M. A.; Cingolani, R.; Cozzoli, P. D. Architectural Control of Seeded-Grown Magnetic-Semicondutor Iron Oxide-TiO(2) Nanorod Heterostructures: The Role of Seeds in Topology Selection. *J. Am. Chem. Soc.* **2010**, *132*, 2437–2464.
66. Habas, S. E.; Yang, P. D.; Mokari, T. Selective Growth of Metal and Binary Metal Tips on CdS Nanorods. *J. Am. Chem. Soc.* **2008**, *130*, 3294–3295.
67. Maynadie, J.; Salant, A.; Falqui, A.; Respaud, M.; Shaviv, E.; Banin, U.; Soulantica, K.; Chaudret, B. Cobalt Growth on the Tips of CdSe Nanorods. *Angew. Chem., Int. Ed.* **2009**, *48*, 1814–1817.
68. Li, X. H.; Lian, J.; Lin, M.; Chan, Y. T. Light-Induced Selective Deposition of Metals on Gold-Tipped CdSe-Seeded CdS Nanorods. *J. Am. Chem. Soc.* **2011**, *133*, 672–675.
69. Jen-La Plante, I.; Habas, S. E.; Yuhas, B. D.; Gargas, D. J.; Mokari, T. Interfacing Metal Nanoparticles with Semiconductor Nanowires. *Chem. Mater.* **2009**, *21*, 3662–3667.
70. Menagen, G.; Mocatta, D.; Salant, A.; Popov, I.; Dorfs, D.; Banin, U. Selective Gold Growth on CdSe Seeded CdS Nanorods. *Chem. Mater.* **2008**, *20*, 6900–6902.
71. Carbone, L.; Kudera, S.; Giannini, C.; Ciccarella, G.; Cingolani, R.; Cozzoli, P. D.; Manna, L. Selective Reactions on the Tips of Colloidal Semiconductor Nanorods. *J. Mater. Chem.* **2006**, *16*, 3952–3956.
72. Figuerola, A.; van Huis, M.; Zanella, M.; Genovese, A.; Marras, S.; Falqui, A.; Zandbergen, H. W.; Cingolani, R.; Manna, L. Epitaxial CdSe-Au Nanocrystal Heterostructures by Thermal Annealing. *Nano Lett.* **2010**, *10*, 3028–3036.
73. Khalavka, Y.; Sonnichsen, C. Growth of Gold Tips onto Hyperbranched CdTe Nanostructures. *Adv. Mater.* **2008**, *20*, 588–591.
74. Chakrabortty, S.; Yang, J. A.; Tan, Y. M.; Mishra, N.; Chan, Y. T. Asymmetric Dumbbells from Selective Deposition of Metals on Seeded Semiconductor Nanorods. *Angew. Chem., Int. Ed.* **2010**, *49*, 2888–2892.
75. O'Sullivan, C.; Gunning, R. D.; Barrett, C. A.; Singh, A.; Ryan, K. M. Size Controlled Gold Tip Growth onto II-VI Nanorods. *J. Mater. Chem.* **2010**, *20*, 7875–7880.
76. Mokari, T.; Rothenberg, E.; Popov, I.; Costi, R.; Banin, U. Selective Growth of Metal Tips onto Semiconductor Quantum Rods and Tetrapods. *Science* **2004**, *304*, 1787–1790.
77. Mokari, T.; Sztrum, C. G.; Salant, A.; Rabani, E.; Banin, U. Formation of Asymmetric One-Sided Metal-Tipped Semiconductor Nanocrystal Dots and Rods. *Nat. Mater.* **2005**, *4*, 855–863.
78. Elmalem, E.; Saunders, A. E.; Costi, R.; Salant, A.; Banin, U. Growth of Photocatalytic CdSe-Pt Nanorods and Nanonets. *Adv. Mater.* **2008**, *20*, 4312–4317.
79. Saunders, A. E.; Popov, I.; Banin, U. Synthesis of Hybrid CdS-Au Colloidal Nanostructures. *J. Phys. Chem. B* **2006**, *110*, 25421–25429.

80. Sobal, N. S.; Ebels, U.; Möhwald, H.; Giersig, M. Synthesis of Core−Shell PtCo Nanocrystals. *J. Phys. Chem. B* **2003**, *107*, 7351–7354.
81. Sobal, N. S.; Hilgendorff, M.; Möhwald, H.; Giersig, M.; Spasova, M.; Radetic, T.; Farle, M. Synthesis and Structure of Colloidal Bimetallic Nanocrystals: The Non-Alloying System Ag/Co. *Nano Lett.* **2002**, *2*, 621–624.
82. Bao, F.; Li, J.-F.; Ren, B.; Gu, R.-A.; Tian, Z.-Q. Synthesis and Characterization of Au@Co and Au@Ni Core−Shell Nanoparticles and Their Applications in Surface-Enhanced Raman Spectroscopy. *J. Phys. Chem. C* **2007**, *112*, 345–350.
83. Sobal, N. S.; Giersig, M. Core-Shell Pd/Co Nanocrystals. *Aust. J. Chem.* **2005**, *58*, 307–310.
84. Kim, B. Y.; Shim, I.-B.; Araci, Z. O.; Saavedra, S. S.; Monti, O. L. A.; Armstrong, N. R.; Sahoo, R.; Srivastava, D. N.; Pyun, J. Synthesis and Colloidal Polymerization of Ferromagnetic Au-Co Nanoparticles into Au-Co_3O_4 Nanowires. *J. Am. Chem. Soc.* **2010**, *132*, 3234–3235.
85. Mokari, T.; Costi, R.; Sztrum, C. G.; Rabani, E.; Banin, U. Formation of Symmetric and Asymmetric Metal-Semiconductor Hybrid Nanoparticles. *Phys. Status Solidi B: Basic Solid State Phys.* **2006**, *243*, 3952–3958.
86. Menagen, G.; Macdonald, J. E.; Shemesh, Y.; Popov, I.; Banin, U. Au Growth on Semiconductor Nanorods: Photoinduced *versus* Thermal Growth Mechanisms. *J. Am. Chem. Soc.* **2009**, *131*, 17406–17411.
87. Park, J.; An, K. J.; Hwang, Y. S.; Park, J. G.; Noh, H. J.; Kim, J. Y.; Park, J. H.; Hwang, N. M.; Hyeon, T. Ultra-Large-Scale Syntheses of Monodisperse Nanocrystals. *Nat. Mater.* **2004**, *3*, 891–895.
88. Tracy, J. B.; Weiss, D. N.; Dinega, D. P.; Bawendi, M. G. Exchange Biasing and Magnetic Properties of Partially and Fully Oxidized Colloidal Cobalt Nanoparticles. *Phys. Rev. B* **2005**, *72*, 064404.
89. Wang, J.; Johnston-Peck, A. C.; Tracy, J. B. Nickel Phosphide Nanoparticles with Hollow, Solid, and Amorphous Structures. *Chem. Mater.* **2009**, *21*, 4462–4467.
90. Railsback, J. G.; Johnston-Peck, A. C.; Wang, J.; Tracy, J. B. Size-Dependent Nanoscale Kirkendall Effect during the Oxidation of Nickel Nanoparticles. *ACS Nano* **2010**, *4*, 1913–1920.
91. Keng, P. Y.; Kim, B. Y.; Shim, I.-B.; Sahoo, R.; Veneman, P. E.; Armstrong, N. R.; Yoo, H.; Pemberton, J. E.; Bull, M. M.; Griebel, J. J.; *et al.* Colloidal Polymerization of Polymer-Coated Ferromagnetic Nanoparticles into Cobalt Oxide Nanowires. *ACS Nano* **2009**, *3*, 3143–3157.
92. Keng, P. Y.; Bull, M. M.; Shim, I.-B.; Nebesny, K. G.; Armstrong, N. R.; Sung, Y.; Char, K.; Pyun, J. Colloidal Polymerization of Polymer-Coated Ferromagnetic Cobalt Nanoparticles into Pt-Co_3O_4 Nanowires. *Chem. Mater.* **2011**, *23*, 1120–1129.
93. Nie, Z. H.; Fava, D.; Kumacheva, E.; Zou, S.; Walker, G. C.; Rubinstein, M. Self-Assembly of Metal-Polymer Analogues of Amphiphilic Triblock Copolymers. *Nat. Mater.* **2007**, *6*, 609–614.
94. Nakata, K.; Hu, Y.; Uzun, O.; Bakr, O.; Stellacci, F. Chains of Superparamagnetic Nanoparticles. *Adv. Mater.* **2008**, *20*, 4294–4299.
95. DeVries, G. A.; Brunnbauer, M.; Hu, Y.; Jackson, A. M.; Long, B.; Neltner, B. T.; Uzun, O.; Wunsch, B. H.; Stellacci, F. Divalent Metal Nanoparticles. *Science* **2007**, *315*, 358–361.
96. Cho, K. S.; Talapin, D. V.; Gaschler, W.; Murray, C. B. Designing PbSe Nanowires and Nanorings through Oriented Attachment of Nanoparticles. *J. Am. Chem. Soc.* **2005**, *127*, 7140–7147.
97. Tang, Z. Y.; Kotov, N. A.; Giersig, M. Spontaneous Organization of Single CdTe Nanoparticles into Luminescent Nanowires. *Science* **2002**, *297*, 237–240.
98. Alemseghed, M. G.; Ruberu, T. P. A.; Vela, J. Controlled Fabrication of Colloidal Semiconductor-Metal Hybrid Heterostructures: Site Selective Metal Photo Deposition. *Chem. Mater.* **2011**, *23*, 3571–3579.
99. Puzder, A.; Williamson, A. J.; Zaitseva, N.; Galli, G.; Manna, L.; Alivisatos, A. P. The Effect of Organic Ligand Binding on the Growth of CdSe Nanoparticles Probed by ab Initio Calculations. *Nano Lett.* **2004**, *4*, 2361–2365.
100. O'Sullivan, C.; Ahmed, S.; Ryan, K. M. Gold Tip Formation on Perpendicularly Aligned Semiconductor Nanorod Assemblies. *J. Mater. Chem.* **2008**, *18*, 5218–5222.
101. Peng, Z. A.; Peng, X. Mechanisms of the Shape Evolution of CdSe Nanocrystals. *J. Am. Chem. Soc.* **2001**, *123*, 1389–1395.